Journal of South American Earth Sciences 129 (2023) 104502

Contents lists available at ScienceDirect

Journal of South American Earth Sciences

journal homepage: www.elsevier.com/locate/jsames

Application of TOPSIS model in active tectonic prioritization: Madeira watershed, South America

Adrija Raha [a], Mery Biswas [a,**], Soumyajit Mukherjee [b,*]

[a] Department of Geography, Presidency University, 86/1 College Street, Kolkata, 700 073, West Bengal, India
[b] Department of Earth Sciences, Indian Institute of Technology Bombay, Powai, Mumbai, 400 076, Maharashtra, India

ARTICLE INFO

Keywords:
Morphometry
TOPSIS
Active tectonics
Geodynamics
Collision zone tectonics
Andean orogeny

ABSTRACT

The Andes orogenic belt is one of the most tectonically active zones located between the convergent margins of the South American plate and the Pacific plate. From the dissected western belt to the expanded alluvial plain of Amazon basin, the Madeira watershed bears recent tectonic imprints. The tectonic signature is well documented by the spatial and linear characteristics of the five sub watersheds along with the Madeira trunk river and channels. The level of tectonic activeness has been assessed on the sub watersheds of the Madeira River, which is one of the main right-hand tributaries of the Amazon River. On the five defined sub-watersheds and the main channel watershed of Madeira, several morphometric indices, viz., asymmetry factor (AF), tilt angle (β), sinuosity index (SI), channel concavity (ϴ), elongation ratio (Re), circularity ratio (Rc), transverse topographic symmetry factor (T) and basin shape index (Bs), have been used. To rank the watersheds based on tectonic activity, we applied the *Technique for Order Preference by Similarity to Ideal Solution* (TOPSIS) The active tectonics was also tested by a comparative study of linear indicators as Hack profiles, longitudinal profiles and segment-wise stream gradient index (SL) of watersheds 2 (rank 1) and 3 (rank 6). The results reveal that the most tectonically active watershed 2 is located in a high seismic magnitude zone with several deep earthquake epicenters. The least tectonically active watershed 6 is located in a low seismic zone.

1. Introduction

Morphometry of terrains includes studies of uplift-incision rates, fault slip rates and neotectonic processes in the recent geologic past (e.g., Doornkamp, 1986; Burbank and Anderson, 2001; Azor et al., 2002; Keller and Pinter, 2002; Bull, 2007; Mahmood and Gloaguen, 2012). Neotectonics help to understand the terrestrial hazards, land-use problems and management of the concerned areas (Pedrera et al., 2009). Rivers being one of most important natural features reflect tectonic sensitivity in terms of their geometries. However, it can often be challenging to determine the influence of neotectonics, as the flow paths of the rivers may be altered by the pre-existing structural and geomorphologic units (e.g., Nag and Chakraborty, 2003; Strecker et al., 2003).

The tectonic control on rivers can be assessed on areal aspects, i.e., on watershed-scale and also on linear-scale. Combinations of factors can be used to interpret the overall idea of the hydrology and morphology of the land surface (Gruber and Peckham, 2009; Olaya, 2009; Florinsky, 2017). The development of morphometric indices using Geographical Information System (GIS) and remote sensing platforms facilitates analyzing diverse geographic data (Remondo and Oguchi, 2009). These methods have aided in quantifying geomorphic characteristics and their pertinent mapping on a range of spatial entities, particularly in river basin studies (Pike, 2000; Evans et al., 2009; Pike et al., 2009).

In the last ten years or so, multi-criteria decision-making models have been used increasingly to determine the tectonic sensitivity of basins. Technique for Order of Preference by Similarity to Ideal Solution (TOPSIS) is one such multi-criteria decision-making model. (Table 1).

Neotectonic deformation localized in the Andes in South America due to the ongoing geodynamic processes (Costa et al., 2020). The Eastern and the Central Cordilleras with the Merida Andes and the Perija Range of Venezuela are parts of the pre-Mesozoic basement, which has been revealed by paleomagnetic studies (Bayona et al., 2006, 2010).

The present study focuses on a cratonic area with slow deformation adjacent to the active Andean deformation front (Mejia, 2011). The Andean chain is characterized by a typical oceanic-continental plate

* Corresponding author.
** Corresponding author.
E-mail addresses: mery.geog@presiuniv.ac.in, merybiswas@gmail.com (M. Biswas), smukherjee@iitb.ac.in, soumyajitm@gmail.com (S. Mukherjee).

https://doi.org/10.1016/j.jsames.2023.104502
Received 26 December 2022; Received in revised form 20 June 2023; Accepted 24 July 2023
Available online 26 July 2023

boundary around its central area, and by the predominance of strike-slip tectonics at the northern and southern portions (Quiero et al., 2022). The South American river systems owing to their origin from the Andes mountain exhibit tectonic imprints (Suvires et al., 2012; Climate Policy Watcher, 2022). One of the major right-hand tributaries of the Amazon River, which rises in the Andes, is the Madeira River. This river has grown into its own channel network, with a few smaller basins (Fig. 1). Geoscientists so far concentrated on the evolution (e.g., Encinas et al., 2021; Quiero et al., 2022) and mineralogy (e.g., Wallace and Hall-Wallace, 2003; Hammarstrom, 2022) of the Amazon cratonic area. However, the application of morphometric indices, and especially the TOPSIS analyses, has not been applied to determine the active tectonics in the considered study area.

This article assesses the tectonic prioritization of sub-watersheds of the Madeira drainage basin based on the morphometric indices applied on both linear and basin-scales. Multi-criteria decision making (MCDM) methods might be effective for ranking the watersheds (Pourghasemi et al., 2021; Kumar and Sarkar, 2022). Tools for such analysis emphasize on obtaining and rating the set of options while taking the criterion into account. The TOPSIS model has been used as an MCDM technique in this study to prioritize the sub-watersheds. TOPSIS is a distance-based method that determines the Euclidian distance from both the positive ideal solution and the negative ideal solution (Hwang and Yoon, 1981; Kumar and Sarkar, 2022).

Earlier studies (Sl 1 to 8 in Table 2) in the surrounding areas were based on neotectonic activities that considered specific watersheds of Madeira. We investigate the relative tectonic activity in the Madeira basin.

Table 1
TOPSIS application in different fields of geographical studies.

Authors	Terrain	Key Methods	Key Conclusion
Aouragh and Essahlaoui (2018)	Oum Er-Rbia basin, Morocco	TOPSIS has been applied encompassing some morphometric parameters to prioritize watersheds for soil and water resource conservation	The GIS and TOPSIS techniques provide accurate result and are simple yet cost effective.
Nitheshnirmal et al. (2019)	Dnyanganga watershed of Tapti River basin, India	The sub-watersheds have been ranked based on TOPSIS-AHP model based on soil erosion potentiality	Soil erosion potentiality assessment.
Bohra and Bhardwaj (2020)	Upper Kosi watershed, India	The sub-watersheds have been ranked based on TOPSIS-AHP model based on soil erosion potentiality	The Upper Kosi watershed contains 4.73, 38.79 and 56.48% of its area in high, medium, and low susceptible zone, respectively
Ghaleno et al. (2020)	Gorganrud River Basin of Golestan province, Iran	TOPSIS, Simple Additive Weighting (SAW), Elimination Et Choice Translation Reality (ELECTRE) and Vise Kriterijumska Optimizacija Kompromisno Resenje (VIKOR) techniques have been applied	The results of different Multi-Criteria Decision Making (MCDM) methods have been compared which shows the SAW model to be most reliable in terms of the conducted study.
Meshram et al. (2020)	Bamhani and Mohgaon watersheds, Mandala district, Madhya Pradesh, India	The considered sub-watersheds have been prioritized based on soil erosion potentiality. Four morphometric parameters have been chosen to perform SAW and TOPSIS model	Potential of soil erosion worked out, important for resource management
Barman et al. (2021)	Chite Lui watershed, India	To identify the soil erosion and ground water potential zone, TOPSIS applied. The parameters have been assigned with weightages by AHP.	TOPSIS has ranked the individual sub-watersheds on the basis of the soil erosion susceptibility and ground water potential zone
Ghosh and Mukhopadhyay (2021)	Dwarkeswar river basin, West Bengal, India	The sub-watersheds have been prioritized based on soil erosion potentiality based on five MCDM techniques- Simple Additive Weighting (SAW), Complex Proportional Assessment (COPRAS), Additive Ratio Assessment (ARAS), TOPSIS, and Multi-Objective Optimization On The Basis Of Ratio Analysis (MOORA).	Complex Proportional Assessment (COPRAS) model has the highest accuracy in the prediction of erosion susceptibility.
Gupta et al. (2021)	Sina river sub-basin, Ahmednagar district, Maharashtra, India	To characterize the sub-watersheds for soil and water conservations in drought prone area with the application of AHP and TOPSIS. Soil & Water Assessment Tool (SWAT) has been applied for the quantitative analysis of surface run off and soil erosion.	Watershed-wise soil and water conservation.
Pourghasemi et al. (2021)	Qareaghaj catchment of Fars Province, Iran	Several Multi-Criteria Decision Making (MCDM) techniques such as weighted aggregated sum product assessment-analytical hierarchy process (WASPAS-AHP) with prevailing benchmark ensemble MCDM models including VlseKriterijumska optimizacija I Kompromisno Resenje (VIKOR)-AHP and TOPSIS-AHP have been applied for ranking sub-watersheds and to determine the most significant parameter influencing water erosion in Qareaghaj catchment	The VIKOR-AHP method gives better result of erosion susceptibility in comparison with the other two methods
Kumar and Sarkar (2022)	Bamni Banjar watershed of Madhya Pradesh, India	Soil erosion vulnerability assessment on sub watershed scale has been performed with the application of AHP and TOPSIS	The morphometric parameters have successfully analyzed the soil erosion potential. AHP has given more accurate result
Patel et al. (2022)	Ami River Basin, Uttar Pradesh, India	The sub-watersheds have been ranked based on TOPSIS-AHP model based on soil erosion potentiality.	The basin has coarse texture of drainage with highly suspect to soil erosion and high run-off
Raha and Biswas (2022)	Jaldhaka river basin, West Bengal, India	TOPSIS applied to identify the most active watershed along with their main channels in terms of tectonism	A comparative analysis has been performed between the alluvial fans formed by the aggradation mechanism of the least active and most active channels. The alluvial fan 2 is seen to be deformed by the Thaljhora thrust. Alluvial fan 3 has been marked with intense sedimentation at its eastern flank by river Rohtikhola.
Sarkar et al. (2022)	Pindar river watershed, Uttarakhand, India	Application of several MCDM viz. AHP, Fuzzy Analytic Hierarchy Process (FAHP), TOPSIS and VIKOR for prioritization of the sub-watersheds based on soil erosion	The evaluation of the MCDM techniques has been executed based on percentage of change and intensity of change. The result shows that FAHP model represents the most accurate result.

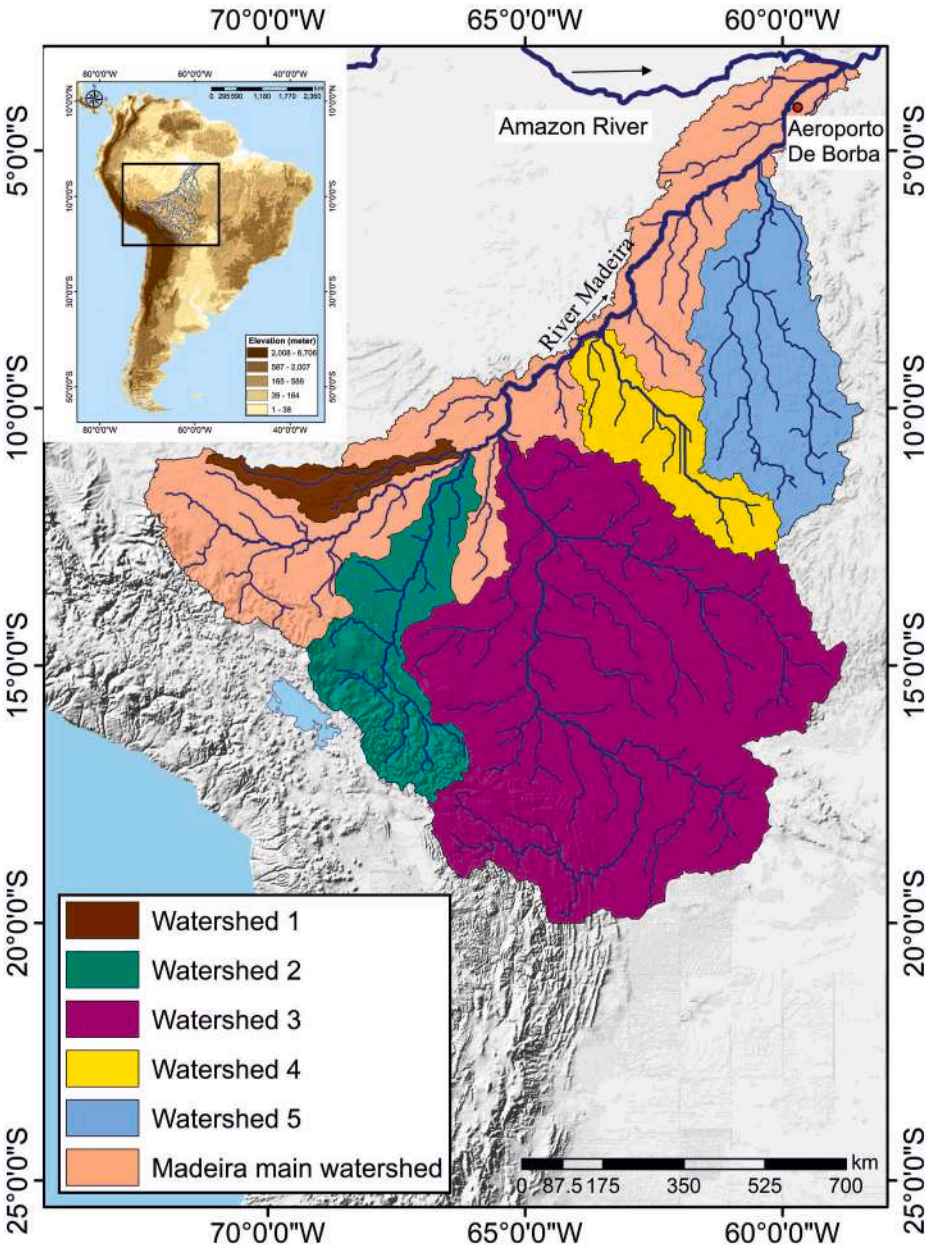

Fig. 1. Madeira watershed with five sub-watersheds and the main channel watershed. Inset map of South America locates Madeira watershed.

2. Geology and tectonics

Converging plates at the subduction zones define a compressional tectonic regime. The shortening reconstruction regarding the collisional tectonics between the Andes with the South America-Antarctica-(Pacific)-Nazca plate circuit. The Nazca plate passed ~1000 km along the trench and subducted since ~11–12 Ma with the onset of flat slab subduction (Schepers et al., 2017). The catchment section of the studied watershed exists between the subduction zone of Peruvian and Pampean flat slab segment of Nazca plate (Schepers et al., 2017) (Fig. 2a). An increase in tectono-magmatic activity occurred due to accelerated convergence during the formation of the Nazca plate and continued as the central and Southern Andean fold-and-thrust belt reconstruction at 50 Ma (Schepers et al., 2017). This was followed by the breakup of the Farallon plate in the Late Oligocene to Early Miocene (Bond et al., 1984). As per the recent high-resolution plate reconstructions (Chatterjee and Mukherjee, 2022), convergence rate varied at the Andean boundary (Quiero et al., 2022). The Andean deformation regime existed for a distance of 12,000 km from northern Venezuela Malvinas Plateau (Mejia, 2011). South America had split from Antarctica as late as the Paleocene (Hay et al., 1999) or the Eocene (Brundin, 1988) or even as early as the Late Jurassic (Smith et al., 1994). Convergent velocity compared to the tectono-magmatic evolution of the Andean margin and the intensification of convergence at 20°S during 15–14 Ma appears to be related to the concurrent activation of fault systems on both edges of the Altiplano (Quiero et al., 2022). Rondonia-San Ignacio (RSI) and Sunsás-Aguapei (SA), the two peripheral provinces (Fig. 2b), produced by accretion and collision during the Mesoproterozoic (Bettencourt et al., 2010).

Paleozoic siliciclastic rocks in the Amazonas Basin is up to 5000 m thick and are intruded by the Mesozoic diabase dikes and sills (Mendes et al., 2015). The Nazca plate, subducting below the South American plate, is located at < 120 km depth beneath most of the Andes. Western Amazonia is typically positioned against eastern Laurentia and Baltica in palaeogeographic reconstructions of the Early Neoproterozoic supercontinent Rodinia (e.g. Hoffman, 1991; Torsvik, 2003; Li et al., 2008).

Table 2
Morphometric works on tectonic of the Andean foreland.

Sl. No.	Author(s)	Terrain	Methodology	Key outcome(s)
1	Gaillardet et al. (1997)	Amazon river basin, South America	Hydro geochemistry and ICP-MS	Drainage for the Solimoes and Madeira rivers, respectively, contains 51% and 18% pure continental crust. The bulk of these drainage basins must therefore contain at least 56% and 18% recycled materials, respectively.
2	Latrubesse et al. (2010)	Amazon river basin, South America	A detailed review of the past researches on the paleontological contents of the Amaon river basin. Facies analysis from river banks and road cuts	Authors dated the Solimes Formation's topmost layers to the Late Miocene in western Amazonia, Brazil. The Huayquerian-Mesopotamian 9 to 6.5 Ma mammalian biozones are designated as the vertebrate fossil record from outcrop. Likewise, they reported deposits in Peruvian Amazonia are actually river deposits
3	Gross et al. (2011)	Solimões Formation, Brazil	Micropalaeontological work carried out. Preliminary stable isotopic studies	The deposits are biostratigraphically dated to be Late Miocene and are a component of the Solimes Formation's upper portion. The presence of the long-lived Lake Pebas or any influx of marine waters for that region during the Late Miocene may be eliminated based on palaeontologic and geologic findings.
4	Pingel et al. (2013)	Eastern Cordillera of NW Argentina, Humahuaca Basin	The tectono-sedimentary history of the southern Humahuaca basin was documented using stratigraphic and structural analysis, detailed geological mapping of exposed units, regional unconformities, sediment provenance, lateral facies pinch-outs and lithological contacts	This basin has been shortening and uplifting. This developed an orographic barrier for moisture-bearing winds from the east along its eastern boundary and led to leeward aridification. Humahuaca basin was a crucial component of a generally continuous depositional system that gradually disconnected from the foreland as deformation progressed eastward from at least 6 Ma until 4.2 Ma. Several cycles of severed hydrological conditions and subsequent re-captured drainage, fluvial connections with the foreland and sediment evacuation occurred
5	Gross and Piller (2018)	Western Amazonia, Peru	By examining the bed thickness, colour, sedimentary formations, grain size, and macrofossil content, the Porvenir section was vertically logged. Under transmitted light, glochidia shells were photographed. Measurements were made of the glochidia's length, height, dorsal hinge line length, and angle of obliquity	The Hyriidae genus Diplodon is presumably the source of these glochidia based on morphologic similarities and the local fossil record. The samples show that such unionid-specific larvae existed in pre-Quaternary eras
6	Mason et al. (2019)	Amazon river basin, South America	Ten samples of fine- to medium-grained sand were taken from turbidite beds in the lower Amazon Fan. Laser ablation-inductively coupled plasma-mass spectrometry and U–Pb dating of zircon grains performed. Kernel density estimates for the resulting DZ ages are shown in their composite stratigraphic context	The authors have pointed out to the interesting finding that, in contrast to the predicted sediment mix found in the lower Amazon today, the Amazon Fan appears to archive a constant record of glacial sea levels and terrestrial hydroclimate of South America
7	Arnous et al. (2020)	Low-Strain Broken Foreland (Santa Bárbara System)	Tectono-geomorphic analysis of the Candelaria Range (CR) piedmonts using digital elevation model, electrical resistivity tomography, seismic-refraction tomography, seismic-reflection stacks and well-log data	Deformation due to regional warping and deep-seated blind thrusting beneath the CR. Layer-parallel folding and flexural-slip faults that cut through Quaternary deposits and landforms at the surface accommodated shortening involving Mesozoic and Cenozoic sedimentary strata in the adjacent basins
8	Lombardo and Grützner (2021)	Bolivian Amazon	A mosaic made of 15 TanDEM-X tiles that covers the centre and northern portions of the LM has been used to dcipher neotectonics	Tectonic block tilted during the Late Pleistocene/Holocene. Tilting can be restored. Risk of catastrophic river course caused by rapid uplift in the low-relief region connote seismic danger
9	Raha et al. (2023; this work)	Madeira watershed, South America	TOPSIS applied to identify the imprint of tectonic activity on the sub-watersheds and main channel watershed of Madeira River. Based on TOPSIS, a comparative analysis has been executed on the most and least active channels	Watershed 2 in the Andean foreland region is more active tectonically. Watersheds in the Amazon cratonic region are less active

Several evidences suggest that Laurentia rifted for the final time in the Late Neoproterozoic. For instance, this is indicated by the stratigraphic change from rift to drift in the Laurentian edge sequences at the Precambrian–Cambrian boundary (e.g. Bond et al., 1984; Williams and Hiscott, 1987). The Andes of Ecuador split into the Eastern Cordillera (the Cordillera Real) and emplaced the Mesozoic plutons with Paleozoic metamorphic pelites and volcanics (Veblen et al., 2007; Pfiffner and Gonzalez, 2013). The Western Cordillera comprises of accreted Late Cretaceous oceanic rocks (Somoza and Ghidella, 2012). The Peruvian Andes is part of the Western Cordillera (the Cordillera Blanca), which is mainly composed of Mesozoic sedimentary rocks, intruded as a Mesozoic arc (the Coastal Batholith) along with younger Tertiary volcanics and localized plutons. The Maranon Complex comprises metasedimentary schists and gneisses that constitute the Eastern Cordillera. Carboniferous and Permo-Triassic plutons are the predominant intrusives (Chew et al., 2008). Broadly, this section is composed of Andean fold belt, Precambrian outcrops and cratonic provinces. (Fig. 2c). In the present plate kinematic framework a few neotectonic events occurred with a rate of ~14 cm y^{-1} in terms of strike-slip faulting of the Andean fold-thrust belt. The convergence rate declined to ~12 cm yr^{-1} at 9 Ma, and remained reasonably stable until 7 Ma. After that the rate significantly reduced to 9 cm yr^{-1} (Quiero et al., 2022).

3. Materials and methods

3.1. Study area

The largest tributary of the Amazon River, the Madeira, drains ~1368290 km^2, covers ~23% of the entire Amazon basin (Guilhen et al., 2022). The Madeira River flows over Bolivia, Peru and Brazil. Nearly 15% of the Amazonian system's total water discharge comes from this river (Júnior et al., 2015; Guilhen et al., 2022). At ~1800 m elevation, Madeira originates close to Guayaramerin, Bolivia. High levels of humidity and precipitation and an average annual rainfall

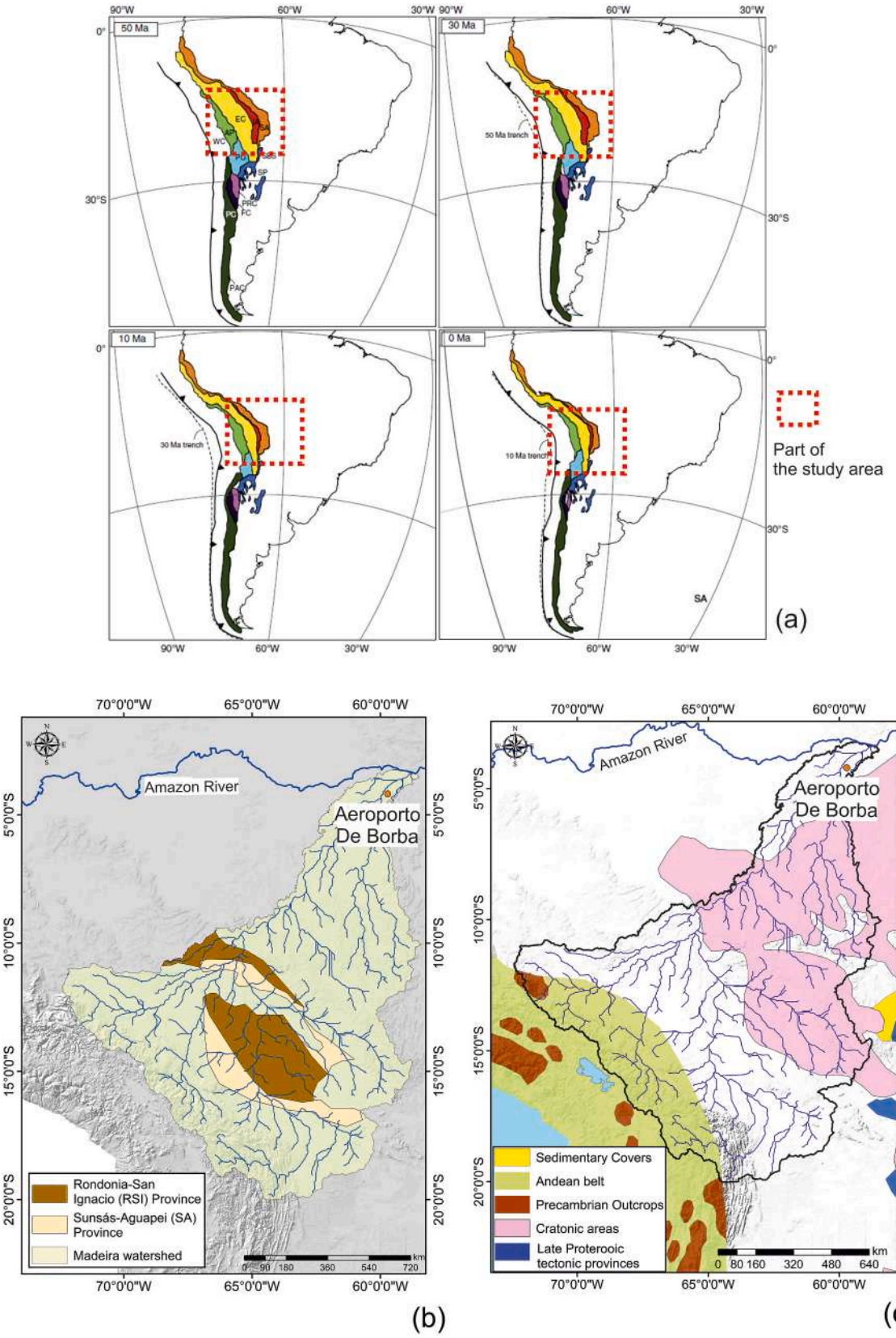

Fig. 2. a. Reconstruction of South America western fixed arc at 50, 30, 10 and 0 Ma. AP, Altiplano Plateau; EC, Eastern Cordillera; FC, Frontal Cordillera; IA, Interandes; AC, Patagonian Cordillera.; PC, Principal Cordillera; PRC, Precordillera; PU, Puna Plateau; SA, Subandes; SBS, Santa Barbara System; SP, Sierras Pampeanas; WC, Western Cordillera (Schepers et al., 2017). **b.** The structural map of the Madeira Basin representing Rondonia-San Ignacio (RSI) and Sunsás-Aguapei (SA), the two peripheral provinces of the region. **c.** Geologic formation from Andean cordillera system to Amazon craton area (Baker et al., 2015).

exceeding 2000 mm characterize the climate. The Andes mountain range, which serves as a source of sediment for the river system and aids in the development of alluvial terraces and floodplains, impacts significantly the geomorphology of the watershed (Veblen et al., 2007).

3.2. Morphotectonic parameters

The main channel watershed of Madeira and its five sub-watersheds were defined and analyzed. Morphometric indices were calculated based on the drainage network extracted from the 30*30 m spatial resolution Digital Elevation Model (DEM). Only streams of third and higher orders were considered in defining the sub-watersheds (Strahler, 1952). Various areal, relief and linear characteristics were evaluated using the ArcGIS version 10.3 (2018). TOPSIS model was applied to rank the watersheds as per their tectonic prioritization. TOPSIS was first proposed as a multi-criteria decision-making technique in 1981 (Hwang and Yoon, 1981; Aouragh and Essahlaoui, 2018). This method determines the alternative closest to the positive ideal solution (PIS). It is most distant to the negative ideal solution (NIS) and ranks the considered regional entity accordingly (Chen, 2000). This model was run based on the following parameters: asymmetric factor (AF), tilt angle (β), sinuosity index (SI), channel concavity (ɵ), elongation ratio (Re), circularity ratio (Rc), transverse topographic symmetry (T) and basin shape (Bs) (Table 1).

3.3. Basin prioritization using TOPSIS

The aforementioned parameters were applied on the five sub-watersheds and on the main watershed of the Madeira basin. Based on the calculated values, the watersheds were ranked to assess the level of tectonic activeness.

In this study, the values of the morphometric indices indicate both ideal and anti-ideal points. The ideal point can be referred to lower values of SI and higher values of AF, which connote tectonic activeness. Higher values of SI and lower values of AF indicating less tectonic activeness can be inferred as anti-ideal point. In this method, the best alternative indicator must have the shortest distance from the positive ideal solute on and the greatest distance from the negative ideal solution. The entire calculations were carried out in Excel (2016) **(Repository 1).** The following steps were performed (Aouragh and Essahlaoui, 2018).

Step 1. Establishment of the decision matrix for ranking (based on the computed parameters) (Aouragh and Essahlaoui, 2018)

A1, A2 … An are possible alternatives. C1, C2 … Cn are the criteria with which the alternative performances are to be measured. Xij is the rating of alternative with respect to criteria.

Step 2. Calculation of the normalized decision matrix.

$$nij = \frac{X_{ij}}{\sqrt{\sum_{i=1}^{x_{ij}} X_{ij}^{\,2}}} \ (equ\ 1)$$

Step 3. Calculation of the weighted normalized

$$v_{ij} = w_j * n_{ij,} \quad i = 1, \ldots, m, j = 1, \ldots, n \ (equ\ 2)$$

The weights were calculated using the Analytic Hierarchic Process (AHP).

Step 4. Identification of the positive ideal (A+) and negative ideal (A-) solutions.

$$A+ = \left(\left(\max_i v_{ij} \middle| j \in J \right), \left(\min_i v_{ij} \middle| j \in J' \right) \middle| i = 1, 2, \ldots, m \right) \ (equ\ 3)$$

$$= \left\{ v_1^+, v_2^+, \ldots, v_m^+ \right\}$$

$$A- = \left(\left(\min_i v_{ij} \middle| j \in J \right), \left(\max_i v_{ij} \middle| j \in J' \right) \middle| i = 1, 2, \ldots, m \right) \ (equ\ 4)$$

$$= \left\{ v_1^-, v_2^-, \ldots, v_m^- \right\}$$

J and J′ are associated with positive and negative criteria, respectively.

Step 5. Calculation of the separation measures by using the n-dimensional Euclidian distance. The separation from each alternative from the ideal solution is:

$$S_i^+ = \sqrt{\sum_{j=1}^{n} \left(v_i^+ - v_{ij} \right)^2} \quad i = 1, 2, \ldots, m \ (equ\ 5)$$

The separation from the negative ideal solution is:

$$S_i^- = \sqrt{\sum_{j=1}^{n} \left(v_i^- - v_{ij} \right)^2} \quad i = 1, 2, \ldots, m \ (equ\ 6)$$

Step 6. Calculation of the relative closeness to the ideal solution.

$$C_i^+ = \frac{S_i^+}{S_i^+ + S_i^-} \ (equ\ 7)$$

3.4. Assessment of linear-scale indicators

After calculating the TOPSIS prioritization model, following the rank of the considered watersheds, the most and the least active watersheds, (i.e., watersheds 2 and 3, respectively), were studied separately to compare the considered linear parameters, viz., longitudinal profile, Hack profile and segment-wise stream gradient index (SL). The longitudinal profile can represent the past and present geomorphic processes. The gradient of river determines the rate of erosion and the depositional character. Abrupt changes in the longitudinal profile along the river indicate the presence of lineaments, faults and knickpoints (Seeber and Gornitz, 1983). Secondly, the Hack profile was applied to determine the nature of the river profiles, which are best understood with the help of semi-logarithmic profiles. In such profiles, the 'X' axis denotes the cumulative distance from the source of river and the 'Y' axis the elevation (Kale, 2010). Rivers exhibit a straight line on a semi-logarithmic graph when in equilibrium. The line signifies radial decrease of channel gradient downstream. Hack (1973) explained the relationship between elevation and channel length. SL provides insight into the control of tectonics and lithology on the longitudinal profiles of the rivers. In the present study, two rivers were divided into ten segments of equal lengths (Fig. 3a). In the areas within a short distance, several uplift episodes increased the SL magnitudes. The SL between two segments of a river was calculated using the formula postulated by Hack (1957) (detail in Table 3).

3.5. Study of seismological data

The seismologic data was considered from 1902 to 2022 and the study was based on the magnitude (mb) of the earthquake with varying depth (km). The data set is based on the United States Geological Survey (USGS) (Internet ref 1).

4. Results

The sub-watersheds of Madeira River and its main watershed are characterized by different degrees of asymmetry, which is reflected in the values of AF. The value of AF is maximum (35.828) for the main

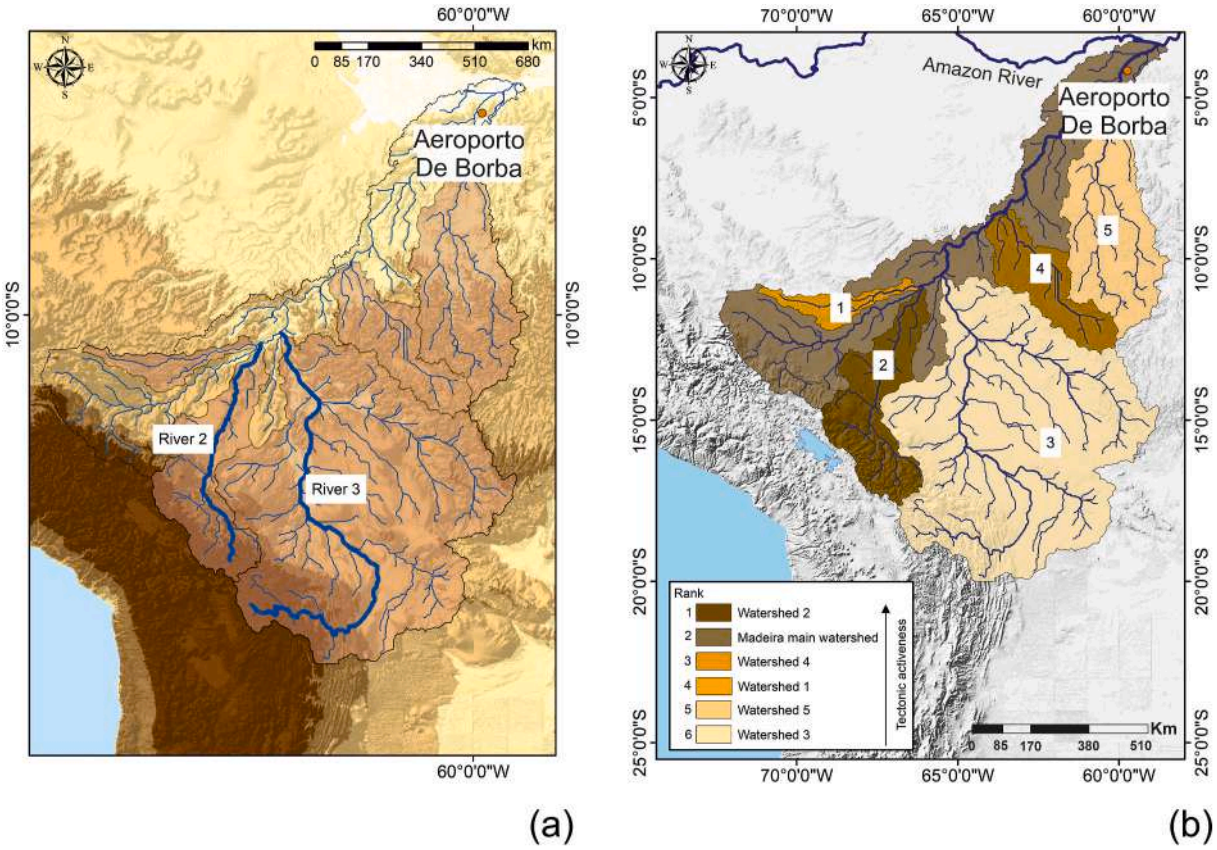

Fig. 3. a. Map of two selected rivers (most active and least active) for linear-scale analysis. **b.** Ranking of the five watersheds and main channel watershed of Madeira according to the TOPSIS model.

Madeira watershed., which is tilted towards south. Additionally, watersheds 1 and 4 are more asymmetric, with higher AF values, 19.126 and 21.727, respectively. Watershed 1 and 2 are is significantly tilted towards southwest and west, respectively. Watershed 3 has the lowest AF = 4.38, which indicates the most symmetric alignment of the river basin with least tilting.

Tilt Angle (β) portrays the degree of tilting of the watersheds. Watershed 2 has the maximum tilting (3.048°), which is followed by the main watershed of Madeira (1.039°). Watershed 3 and 4 have almost similar degree of tilting, 0.789° and 0.728°, respectively. For watershed 1, β = 0.170°. This indicates the least amount of tilting of the watershed.

The sinuosity values show how differently the channels have responded to the tectonic effects. Rivers 1 and 4 (Fig. 1) run mostly straight, with SI values of 1.175 and 1.187, respectively. River 3 with maximum meandering has the higher SI value = 1.997. The main channel of Madeira also meanders with SI value of 1.342. The channel concavity (ɵ) differs amongst the considered channels because of the diverse structural and lithologic control.

Rivers 1 and 4 have extremely low concavity, 0.117 and 0.170, respectively. The Madeira main channel and river 3 exhibit moderate concavity (0.543 and 0.682, respectively). The Elongation Ratio (Re) value is the lowest (0.517) for watershed 1. Watersheds 4 and 5 have same value of Re = 0.572 signifying their elongated nature. Maximum value of Re = 0.832 has been found for watershed 3, which suggests a circular shape of the watershed.

Circularity Ratio (Rc) is minimum (0.194) for watershed 1, which is laterally less extended. The highest Rc (0.392) is from the watershed 3, which has a more rounded form. Watersheds 2 and 4 have Rc values of 0.277 and 0.274, respectively, signifying their elongated shapes, which expanded laterally. Due to its elongated structure, watershed 1 has the highest Basin Shape index (Bs) value of 3.043. Watershed 5 also portrays an elongated shape in terms of its Bs value of 2.844. Bs value of Watershed 3 (1.159) indicates a rounded shape of the watershed, which has extended laterally significantly. The values of Transverse Topographic Symmetry Factor (T) throws some light of the deviation of the main channels from the mid-path of their respective watersheds. It has been noted that the value of T is maximum (0.756) for watershed 1. Its magnitude is minimum for watershed 2 (0.307).

Based on the calculated parameters, the TOPSIS model has been developed. Analytic Hierarchic Process (AHP) has been adopted to assign weights to the considered parameters. The same has been considered for the TOPSIS model. The TOPSIS model ranks the watershed 2 as the most tectonically active, while the watershed 3 is ranked as the least active (Fig. 3b). The main channel watershed of Madeira attained rank 2 as per the TOPSIS model.

A comparative analysis was made between the tectonic activeness of the most and least active watersheds. This comparison is better indicated by the Hack profiles (Fig. 4a and b). The Hack profile of river 2 exhibits a strongly convex profile towards the middle to downstream segment (Fig. 4a). The downmost section of river 2 (Fig. 4a) displays lesser gradient with a lower SL = 171.87. The Hack profile of river 3 exhibits a lower convexity (Fig. 4b). The longitudinal profile of river 2 shows a considerable convex and steep geometry up to ~200 km length from its source. Four knickpoints were identified along the long profile (Fig. 4b), that are relevant to the uplift/incision mechanism. Stream length gradient index suddenly changes from 702.98 to 1103.72 after crossing the knickpoints (Fig. 5a). The sudden increase of SL values (171.87) for river 2 in the downstream section has also been noted. The longitudinal profile of river 3 is overall concave (Fig. 5b). Three knickpoints were identified in river 3 (Figs. 3–5).

Table 3
Considered geomorphic parameters.

Sl. No.	Formula for basin scale indicators	Equations & meaning of symbols	Explanations	References
1	Asymmetry Factor (AF)	$AF = \left(\frac{A_r}{A_t}\right) * 100$ A_r: area of the basin (km^2) to the right of the main channel facing downstream and A_t: total area (km^2) of the basin.	An indicator to measure how much a river basin is tilted due to tectonics. Tectonic activity causes the main stream to change course, sloping away from the basin's midline	Hare and Gardner (1985); e.g. Anand and Pradhan (2019)
2	Tilt Angle (β)	$\beta = \arccos\left[\left\{\left(\frac{b}{a}\right)^2 sin^2\,\alpha + cos^2\,\alpha\right\}^{0.5}\right]$ A: the depositional slope of the basin, a: half-length of major axis, b: half-length of minor axis.	A basin can be thought of as a symmetric topographic entity with topographic features on the surface creating concentric circles when tilting is absent. However, if there is tilting, the surface contours will resemble segments of ellipses with their long axes paralleling tilt direction.	Pinter and Keller (1995); e.g. Mandal and Sarkar (2016)
3	Sinuosity Index (SI)	$SI = \frac{CL}{Vl}$ CL: channel length between two points on a river, : the valley length.	Sinuosity, a measure of a channel's degree of meandering, is used to identify the different geomorphological river types.	Brice (1964)
4	Channel Concavity(ɵ)	$S = ksA^{-\theta}$ S: channel slope, ks: steepness index, 'a' is the concavity index.	Channel concavity explain the differential rates of uplift and erosion. The concept was developed as a relationship between slope and area. Whipple (2004) categorized concavity (ɵ) into four types: i) low concavity (<0.4) is related to short, steep drainage dominated by debris flow, ii) moderate concavity (0.4–0.7) is associated with actively uplifting bedrock channel, iii) high concavity (0.7–1) is related to decrease in the uplift, and iv) extremely high concavity (>1) denotes a transition from incisive to depositional conditions	Hack (1957); e.g. Lee and Tsai (2009)
5	Elongation Ratio (Re)	$Re = 1.128\sqrt{\frac{A}{L_b}}$ A: signifies the area of the basin, Lb: denotes the length of the basin.	Elongation ratio is influenced by geology and climate. The values vary from 0 to 1 (e.g. Wołosiewicz, 2018). As the landscape evolves, the river basin becomes circular and the value tends to be 1.	Schumm (1956); e.g. Wołosiewicz (2018)
6	Circularity Ratio (Rc)	$Rc = \frac{4\pi A}{P^2}$ P: indicates the perimeter of river basin; A: signifies the area of the basin	Circularity ratio of the river basin is influenced by the geologic structures, stream length and frequency, slope and climate. High values indicate the circular shape of the basin indicating the landscape to be mature	Horton (1945)
7	Transverse topographic symmetry (T)	$T = \frac{Da}{Dd}$ Da: the distance from the drainage basin's midline to the meander belt's midline Dd: the distance from the basin's midline to the basin divide.	T in a perfectly symmetric basin has a value of zero. As asymmetry develops, T likewise rises and eventually reaches a value of one. For various lengths of stream channels, the transverse topographic symmetry factor is computed and reveals the stream's preferred migration direction perpendicular to the drainage axis.	Cox (1994)
8	Basin Shape (Bs)	$Bs = \frac{Bl}{Bw}$ Bl: measured length from headwater to the point on the mouth of the basin, Bw: measured width at the widest point on the basin.	In the tectonically active area, the basin tends to be elongated.	E.g. Ramírez-Herrera (1998); Bull &McFadden (1977); Anand& Pradhan (2019)

Sl. No.	**Linear-scale indicators**	**Equations & meaning of symbols**	**Explanations**	**Reference**
1	Long Profile analysis	Linear function y = ax + b Longarithmic function $y = aln[x + b]$ y: elevation (H/H_0); H: elevation of each point, H_0: elevation of the source), x: length of the river (L/L_0); L: distance of the point from the source, L_0: total length of the stream), a, b: coefficients derived independently from each profile.	Long profile denotes the break of slope and formation of knickpoints due to tectonics and lithology from source to mouth.	e.g. Seeber and Gornitz (1983); Biswas et al. (2022a)
2.	Hack Profile	$H = C - k * lnL$ H: altitude of the profile, c: constant. k: SL index, L: stream length measured from the drainage divide at the source of the longest stream in the drainage basin.	On a graph paper with a semi-log scale, rivers in equilibrium appear as straight lines indicating a progressive downstream drop in channel slope. River segments above equilibrium show conditions above grade (i.e. in a high energy state promoting greater erosion and downcutting). The river segments below equilibrium indicate below-grade conditions that encourage deposition.]	Hack (1957) e.g. Kale (2010)
3.	Stream –length Gradient index (SL)	$SL = \frac{h_1 - h_2}{[\ln(d_2) - \ln(d_1)]}$ h_1, h_2: height of the first and second point from the source, respectively; d_1, d_2: distance of first and second point from the source, respectively.	Higher SL values indicate the crossing points of major faults and lineaments both in across and along and lower the values denote fractures and small-scale lineaments.	Hack (1957); e.g. Seeber and Gornitz (1983); Bishop et al. (1985); Goldrick and Bishop (1995); Goldrick and Bishop (2007); Lee and Tsai (2009); Biswas et al. (2022b).

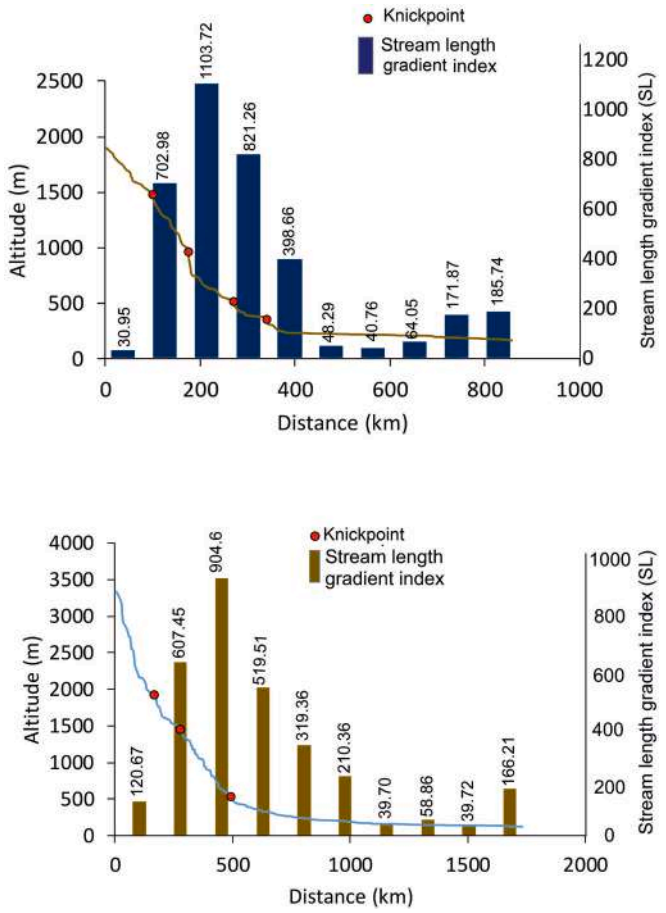

Fig. 4. Hack profiles showing the shape of rivers. a. Convex shape of river 2 (rank 1). b. Comparatively less convex shape of river 3 (rank 6).

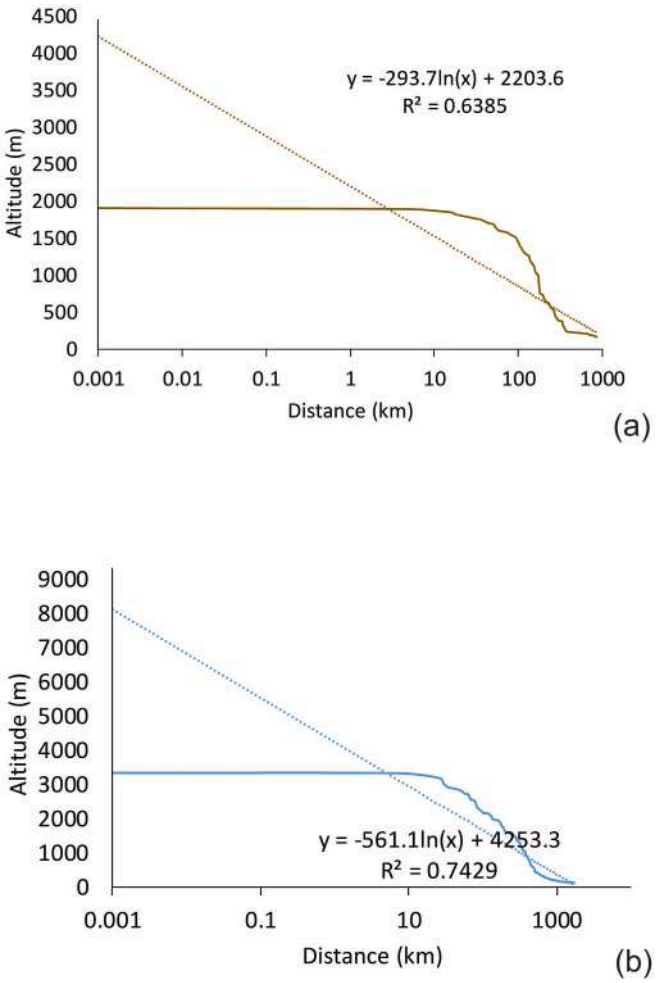

Fig. 5. Longitudinal profile of the most and least active rivers. **5a.** Longitudinal profile of river 2 with the identification of four tectonic knickpoints. Segment wise representation of SL values that connect tectonic control on channel behavior with the existence of knickpoints and higher SL values (1103.72). b. Longitudinal profile of river 3 with identification of three tectonic knickpoints. Segment wise representation of SL values represents comparatively lesser gradient (904.6).

5. Discussions

The study area consists of two unique geomorphic units- *(i)* the western section, which is a segment of the Andean Cordillera system; and *(ii)* the central-eastern part-a portion of the Amazon cratonic basin. The morphometric parameters under consideration indicate the level of tectonic activity. AF in the Madeira main channel watershed can be related to the general slope of the area, which follows from south-west towards north. Due to Madeira's tilt towards the north, its major tributaries flow into its right bank. Yet, due to tectonic and structural control, the watersheds exhibit variable degrees of asymmetry. The tilt angle has often followed the local gradient of the terrain (Fig. 6). The highest tilting is seen in watershed 2. Its catchment area is primarily in the Andes orogenic province with a moderate gradient of $\sim 30^0$. Due to their structural origin and symmetry (T and AF magnitudes in Repository Table 1, step 1), watersheds 3–5 are less tilted because those are located inside the cratonic region. The Andes Orogenic belt is the source of Rivers 1 and 2, which have sharply merged to the foothill region and attained straight to sinuous courses. On the other hand, River 3 has entirely a meandering track while flowing through gently rolling terrain. Because of the gentle topographic gradient that it runs across, River 3 has a greater degree of concavity. The shapes of the basins in terms of Re, Rc and Bs indicate that the watersheds are more elongated in areas with higher altitude, e.g., the Andean foreland region. The main river of watershed 3 is connected by several tributaries and has established a well-developed drainage system, producing a sub-rounded watershed.

TOPSIS model enabled prioritization of watersheds based on tectonic imprints on them. Some studies (e.g., Kale et al., 2014) have already employed the Index of Active Tectonics (IAT) extensively to categorize the sub-watershed depending on its tectonic activeness from different terrains of the world. TOPSIS can be an effective tool in this regard to rank the individual sub-watersheds. It should be mentioned that the sub-watersheds can be categorized/grouped according to their relative activeness level based on the performance score calculated via TOPSIS. The computation techniques are simple. TOPSIS is logical and comprehensible (Kumar and Sankar, 2014) as the idea allows for the pursuit of the best alternatives for each criterion to be represented in a basic mathematical form.

The TOPSIS approach however has certain downsides. For example, TOPSIS can reverse ranks (García-Cascales and Lamata, 2012). When an alternative is added to or removed from the process, it can lead to total rank reversal, when the order of preferences is completely flipped and the option that was previously thought to be the best now is presented as the worst (Wang and Luo, 2009).

The main channels of the most active (watershed 2) and least active (watershed 3) watersheds have been analyzed through linear parameters. The knickpoints on Rivers 2 and 3 are marked within 500 km from the sources of these rivers. This can be attributed to the rugged terrain of the Andean belt. This zone is demarcated as the Andean Deformation

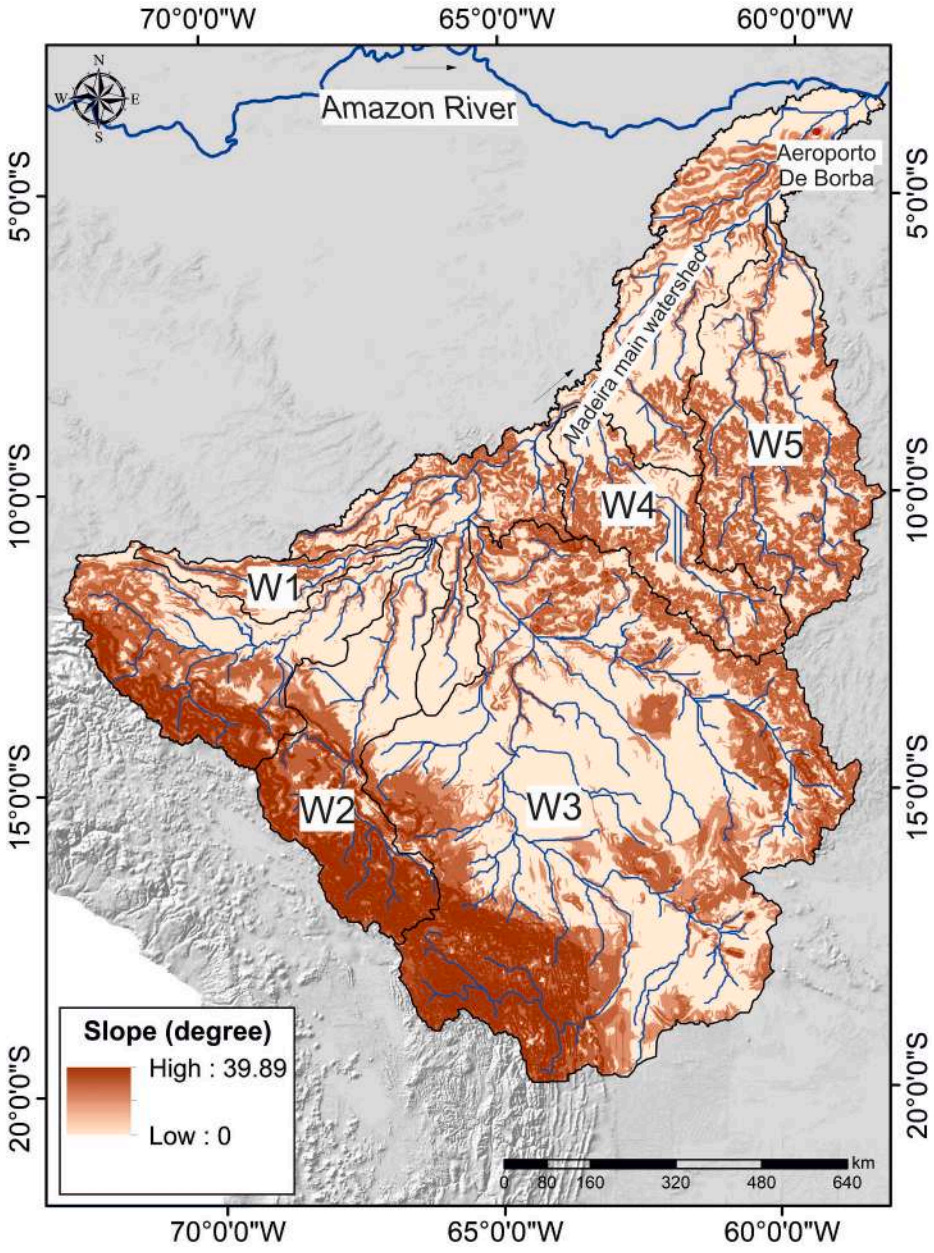

Fig. 6. The slope map of the region showing the variation of gradient (degree).

Zone (Baker et al., 2015) (Fig. 2b). The SL value is maximum for River 2 at ~240 km from its source. The lower reaches of both River 2 (watershed 2) and River 3 (watershed 3) flow over sedimentary cover.

Lower SL values (40.76–64.05 for River 2 and 39.70–58.86 for River 3) in their lower reaches have been documented. Since lithology in the study region is uniform (Fig. 7a), the origin of the knickpoints may be attributed to tectonics. Knickpoints of both Rivers 2 and 3 lie east of the active plate margin (Fig. 7b), which is disturbed by occasional seismic activity. However, their Hack profiles reveal that in the mid-reaches both the rivers display a concave-down/convex nature. The magnitude of convexity is greater for River 2 greater than River 3. Channels have their own structural control and on the areal-scale the watersheds display tectonic imprints.

The main channel of Madeira is comparatively active as it has rank 2 and it flows from the wester Andean fold belt towards the eastern Amazon rift basin. The main channel crosses three major tectonic units-Andean deformation front, Iquitos arc and Purus arc. The Paleozoic and Mesozoic strata overlying the crystalline basement are affected by large-scale folds and thrusts having a trend from north-west to south east (Pfiffner et al., 2013). Thrusts affected the underlying crystalline basement. Seismologic map (Fig. 8) reveals that watershed 2 falls under high seismic zone with several deep-seated earthquake epicenters, which frequently disturbed in the region in the recent past. On the other hand, watershed 3 is a low seismic zone. Though several earthquake epicenters have been found here, the seismic magnitudes are quite low (3.1–4.52 mb). A small portion of watershed 3 lies in the active plate margin and displays few seismic events. However, this watershed lies mostly in the stable cratonic part of Amazon. Watershed 3 is relatively less active in terms of basin and relief parameters.

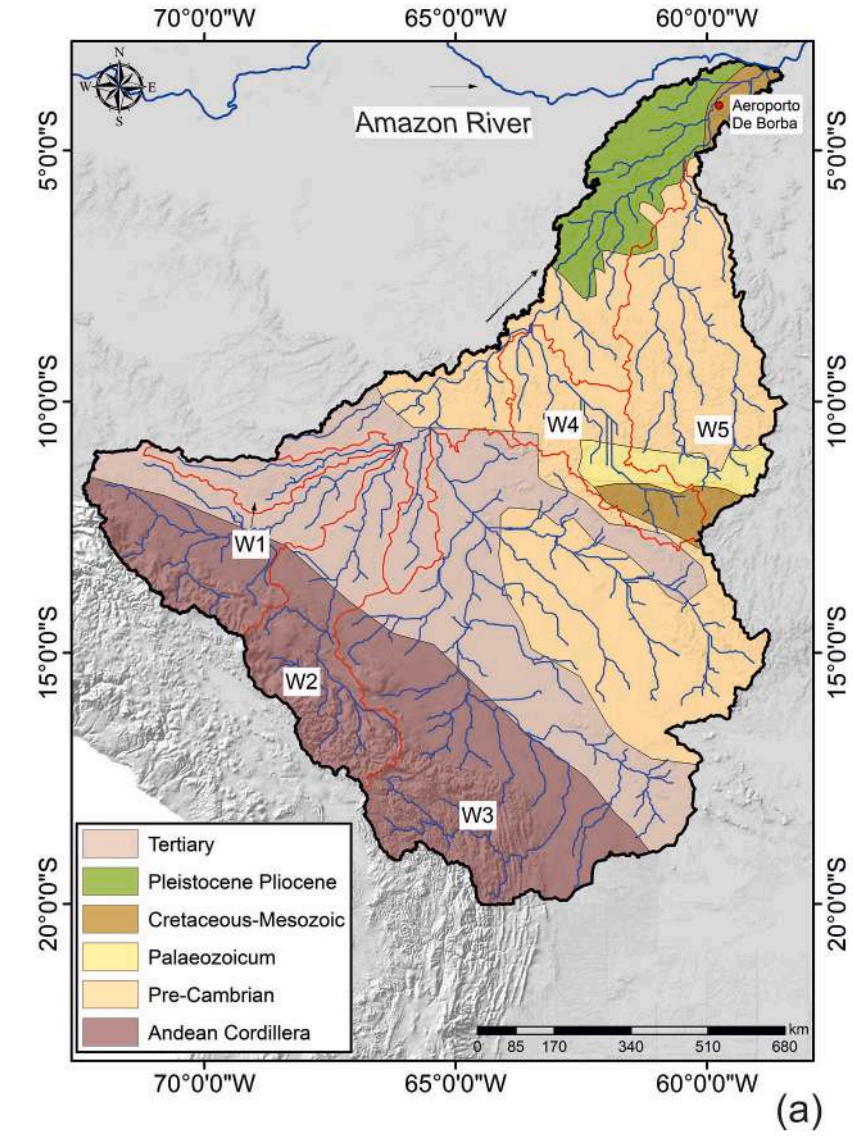

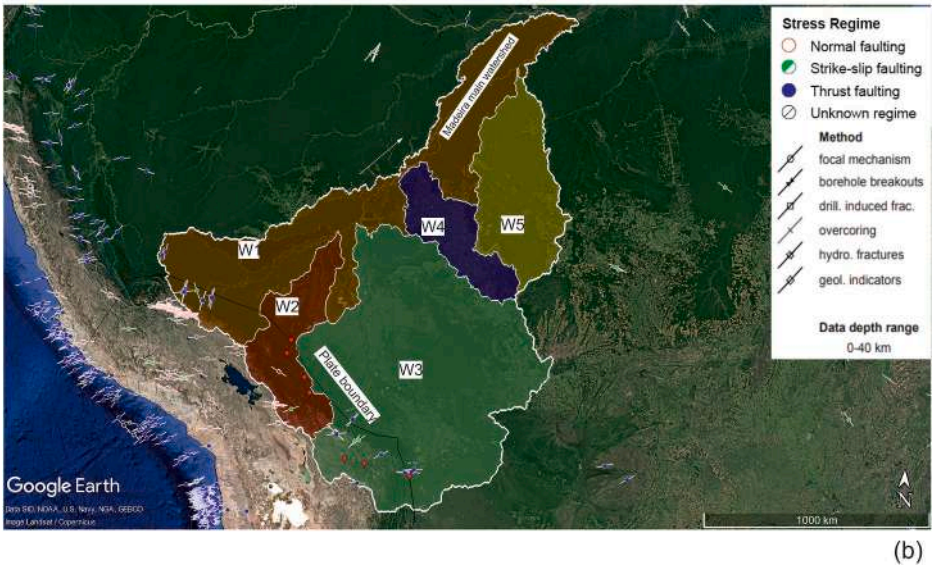

Fig. 7. a. The lithology map of the region presenting six distinct type of lithological units (Piedade et al., 2010). b. Stress map of the region showing the active plate margin. The knickpoints of the considered two rivers (River 2 and 3) have been plotted in white boxes. (Heidbach, Rajabi, Reiter and Ziegler, 2016). (World Stress Map. Home. Retrieved March 1, 2023, from Internet ref-2).

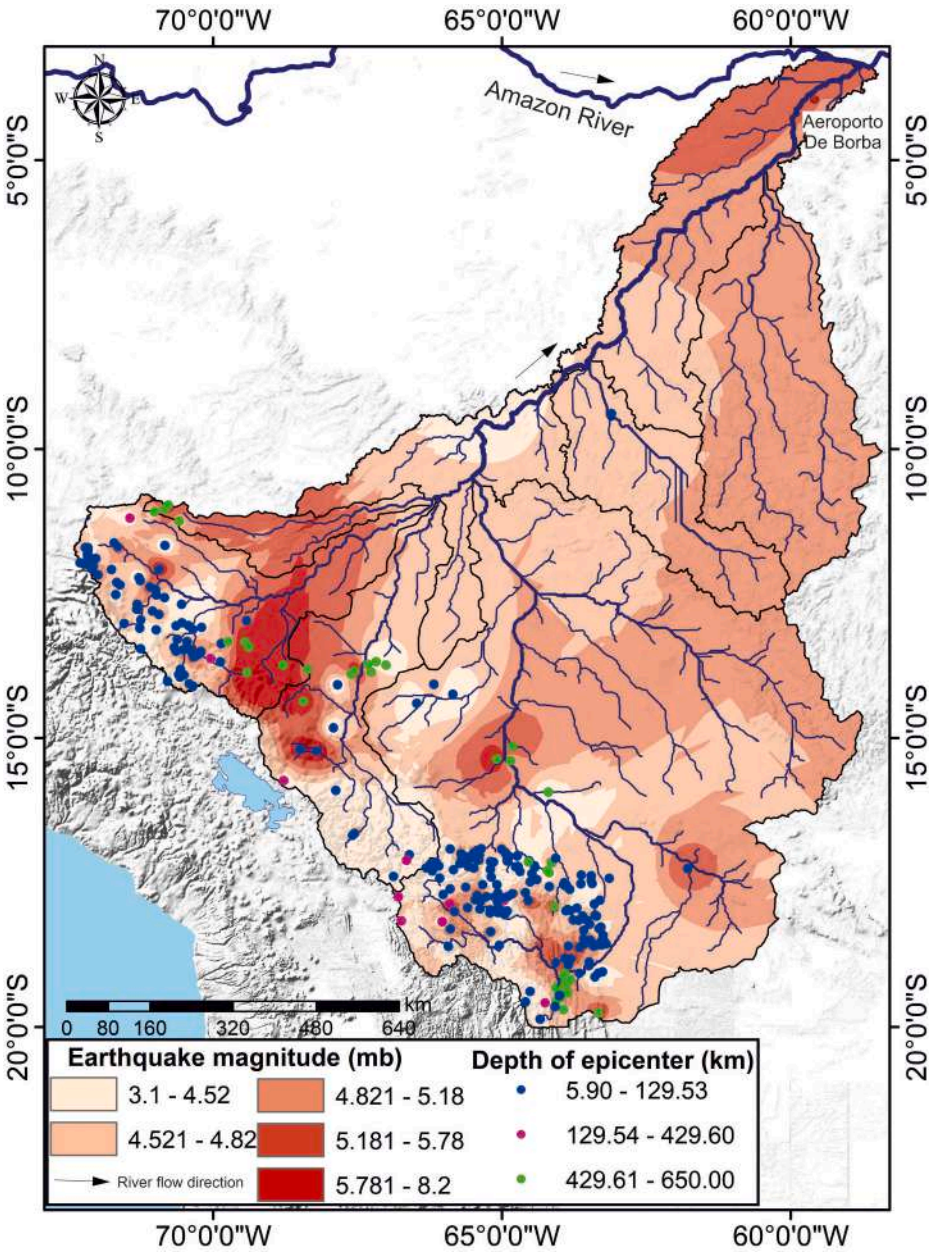

Fig. 8. Seismologic map of the study area with the areal coverage of different seismic magnitude (mb) ranging from 3.1 to 8.2 and the depth (km) of the epicenters classed into three classes and plotted accordingly using different colours (Internet ref .1).

6. Conclusions

The study area has experienced severe tectonic episodes over time. The western Andean fold belt is mostly active. This high activity has controlled the drainage orientation of the upper catchment section passively. Watersheds with assigned ranks 1 to 6 give an idea of tectonic activity, which is based on selected morphometric indices. The tilting of the watersheds has resulted in varied level their asymmetry. The elongated shapes of the watershed 1, 2 and 4 signify the younger stage of their development. The rugged terrains of watersheds 1 and 2 are still undergoing gradational processes. Watershed 5 has approached the mature development stage, which can be inferred from its oval shape and the stream network. The old stage of development is apparent from the circular shape of watershed 3. The flat topography of watershed 3 has been drained by well-developed stream network of various orders. Seismologic data also indicate the western fold belt to be more active than the eastern Amazon cratonic section.

CRediT authorship contribution statement

Adrija Raha: Formal analysis, Data curation. **Mery Biswas:** Writing – original draft, Data curation, Conceptualization. **Soumyajit Mukherjee:** Writing – review & editing, Supervision, Project administration, Funding acquisition.

Declaration of competing interest

We have no conflict of interest. This statement is to certify that all Authors have seen and approved the manuscript being submitted. This research has not been submitted for publication nor has it been published in whole or in part elsewhere.

Data availability

Data will be made available on request.

Acknowledgements

Patricia Ciccioli invited to contribute. CPDA grant (IIT Bombay) supported SM. Chief Editor, Associate Editor and anonymous reviewers provided comments.

Abbreviations and Symbols

AF	Asymmetry Factor
ARAS	Additive Ratio Assessment
Bs	Basin Shape Index
COPRAS	Complex Proportional Assessment
DEM	Digital Elevation Model
ELECTRE	Elimination Et Choice Translation
Ma	Mega annum
MCDM	Multi-criteria decision making
MOORA	Multi-Objective Optimization on the Basis of Ratio Analysis
NIS	Negative Ideal Solution
ɵ	Channel Concavity
PIS	Positive Ideal Solution
Rc	Circularity Ratio
Re	Elongation Ratio
SAW	Simple Additive Weighting
SI	Sinuosity Index
SL	Stream –length Gradient index
T	Transverse topographic symmetry factor
TOPSIS	Technique for Order of Preference by Similarity to Ideal Solution
VIKOR	RealityVise Kriterijumska Optimizacija Kompromisno Resenje
W	Watershed
WASPAS-AHP	Weighted Aggregated Sum Product Assessment-Analytical Hierarchy Process
β	Tilt Angle

References

Anand, A.K., Pradhan, S.P., 2019. Assessment of active tectonics from geomorphic indices and morphometric parameters in part of Ganga basin. J. Mt. Sci. 16 (8), 1943–1961. https://doi.org/10.1007/s11629-018-5172-2.

Aouragh, M.H., Essahlaoui, A., 2018. A TOPSIS approach-based morphometric analysis for sub-watersheds prioritization of high Oum Er-Rbia basin, Morocco. Spatial Info. Res. 26 (2), 187–202. https://doi.org/10.1007/s41324-018-0169-z.

Arnous, A., Zeckra, M., Venerdini, A., Alvarado, P., Arrowsmith, R., Guillemoteau, J., Landgraf, A., Gutiérrez, A., Strecker, M.R., 2020. Neotectonic activity in the low-strain broken foreland (Santa bárbara system) of the north-western argentinean Andes (26°S). Lithosphere, 8888588. https://doi.org/10.2113/2020/8888588, 2020.

Azor, A., Keller, E.A., Yeats, R.S., 2002. Geomorphic indicators of active fold growth: south Mountain–Oak Ridge anticline, Ventura basin, southern California. Geol. Soc. Am. Bull. 114 (6), 745–753. https://doi.org/10.1130/0016-7606(2002)114<0745:gioafg>2.0.co.

Baker et al, 2015. Trans-Amazon Drilling Project (TADP): origins and evolution of the forests, climate, and hydrology of the South American tropics. Sci. Drill. 20, 41–49. https://doi.org/10.5194/sd-20-41-2015.

Barman, B.K., Rao, C.U.B., Rao, K.S., Patel, A., Kushwaha, K., Singh, S.K., 2021. Geomorphic analysis, morphometric-based prioritization and tectonic implications in chite lui river, northeast India. J. Geol. Soc. India 97 (4), 385–395. https://doi.org/10.1007/s12594-021-1696-0.

Bayona, G., Jiménez, G., Silva, C., Cardona, A., Montes, C., Roncancio, J., Cordani, U., 2010. Paleomagnetic data and K–Ar ages from Mesozoic units of the Santa Marta Massif: a preliminary interpretation for block rotation and translations. J. S. Am. Earth Sci. 29 (4), 817–831. https://doi.org/10.1016/j.jsames.2010.02.001.

Bayona, G., Rapalini, V., Constanzo-Alvarez, V., 2006. Paleomagnetism in Mesozoic rocks of the northern Andes and its implications in Mesozoic tectonics of northwestern South America. Earth Planets Space 58, 1255–1272. https://doi.org/10.1186/BF03353370.

Bettencourt, J.S., Barbosa Leite, W., Salina Ruiz, A., Matos, R., Leonelo Payolla, B., Tosdal, R.M., 2010. The rondonian-san Ignacio province in the SW amazonian craton: an overview. J. S. Am. Earth Sci. 29 (1), 28–46. https://doi.org/10.1016/j.jsames.2009.07.006.

Bishop, P., Young, R.W., McDougall, I., 1985. Stream profile change and longterm landscape evolution: early miocene and modern rivers of the east Australian highland crest, central new south wales, Australia. J. Geol. 93 (4), 455–474. https://doi.org/10.1086/628966.

Biswas, M., Gogoi, M.P., Mondal, B., Sivasankar, T., Mukherjee, S., Dasgupta, S., 2022a. Geomorphic assessment of active tectonics in Jaisalmer basin (western Rajasthan, India). Geocarto Int. https://doi.org/10.1080/10106049.2022.2066726.

Biswas, M., Puniya, M.K., Gogoi, M.P., Dasgupta, S., Mukherjee, S., Kar, N.R., 2022b. Morphotectonic analysis of petroliferous Barmer rift basin (Rajasthan, India). J. Earth Syst. Sci. 131, 140. https://doi.org/10.1007/s12040-022-01871-8.

Bohra, B.M., Bhardwaj, A., 2020. Watershed Prioritization of Upper Kosi Watershed Based on Soil Erodibility Computed through TanDEM-X DEM and TOPSIS-AHP Ensemble Model.

Bond, G.C., Nickeson, P.A., Kominz, M.A., 1984. Breakup of a supercontinent between 625 Ma and 555 Ma: new evidence and implications for continental histories. Earth Planet Sci. Lett. 70 (2), 325–345. https://doi.org/10.1016/0012-821x(84)90017-7.

Brundin, L., 1988. Phylogenetic biogeography. In: Myers, A.A., Gillers, P.S. (Eds.), Analytic Biogeography: an Integrated Approach to Plant and Animal Distributions. Chapman Hall, pp. 67–87.

Bull, W.B., 2007. Tectonic Geomorphology of Mountains. A New Approach to Paleoseismology. Wiley-Blackwell. https://doi.org/10.1604/9781405154796.

Bull, W.B., McFadden, L.D., 1977. Tectonic geomorphology north and south of the garlock fault, California. In: Doehring, D.O. (Ed.), Geomorphology in Arid Regions: A Proceedings Volume of the 8th Annual Geomorphology Symposium, vols. 23–24. State University of New York, Binghamton, pp. 115–138.

Burbank, D.W., Anderson, R.S., 2001. Tectonic Geomorphology. Blackwell Science.

Chatterjee, S., Mukherjee, S., 2022. Overview on GPlates: focus on plate reconstruction. Turk. J. Earth Sci. 31, 113–136.

Chen, C.T., 2000. Extensions of the TOPSIS for group decision-making under fuzzy environment. Fuzzy Set Syst. 114 (1), 1–9. https://doi.org/10.1016/s0165-0114(97)00377-1.

Chew, D., Magna, T., Kirkland, C., Miskovic, A., Cardona, A., Spikings, R., Schaltegger, U., 2008. Detrital zircon fingerprint of the Proto-Andes: evidence for a Neoproterozoic active margin? Precambrian Res. 167 (1–2), 186–200. https://doi.org/10.1016/j.precamres.2008.08.002.

Climate Policy Watcher, 2022. Andes tectonic zonation - plate tectonics - climate policy watcher. Retrieved from. https://www.climate-policy-watcher.org/plate-tectonics/andes.html.

Costa, C., Alvarado, A., Audemard, F., Audin, L., Benavente, C., Bezerra, F.H., Garro, H., 2020. Hazardous faults of South America; compilation and overview. J. S. Am. Earth Sci. 104, 102837 https://doi.org/10.1016/j.jsames.2020.102837.

Cox, R.T., 1994. Analysis of drainage-basin symmetry as a rapid technique to identify areas of possible Quaternary tilt-block tectonics: an example from the Mississippi Embayment. Geol. Soc. Am. Bull. 106 (5), 571–581. https://doi.org/10.1130/0016-7606(1994)106<0571:aodbsa>2.3.co.

Doornkamp, J.C., 1986. Geomorphological approaches to the study of neotectonics. J. Geol. Soc. 143 (2), 335–342. https://doi.org/10.1144/gsjgs.143.2.0335.

Encinas, A., Sagripanti, L., Rodríguez, M.P., Orts, D., Anavalón, A., Giroux, P., Valencia, V., 2021. Tectonosedimentary evolution of the coastal cordillera and central depression of South-Central Chile (36° 30′-42° S). Earth Sci. Rev. 213, 103465 https://doi.org/10.1016/j.earscirev.2021.103465.

Evans, I.S., Hengl, T., Gorsevski, P.V., 2009. Applications in geomorphometry. Dev. Soil Sci. 33, 497–525. https://doi.org/10.1016/S0166-2481(08)00022-6.

Florinsky, I.V., 2017. An illustrated introduction to general geomorphometry. Prog. Phys. Geogr. Earth Environ. 41 (6), 723–752. https://doi.org/10.1177/0309133317733667.

Gaillardet, J., Dupre, B., Allegre, C.J., Négrel, P., 1997. Chemical and physical denudation in the Amazon River basin. Chem. Geol. 142 (3–4), 141–173.

García-Cascales, M.S., Lamata, M.T., 2012. On rank reversal and TOPSIS method. Math. Comput. Model. 56 (5–6), 123–132. https://doi.org/10.1016/j.mcm.2011.12.022.

Ghaleno, M.R.D., Meshram, S.G., Alvandi, E., 2020. Pragmatic approach for prioritization of flood and sedimentation hazard potential of watersheds. Soft Comput. 24 (20), 15701–15714. https://doi.org/10.1007/s00500-020-04899-4.

Ghosh, B., Mukhopadhyay, S., 2021. January). Erosion susceptibility mapping of sub-watersheds for management prioritization using MCDM-based ensemble approach. Arabian J. Geosci. 14 (1) https://doi.org/10.1007/s12517-020-06297-4.

Goldrick, G., Bishop, P., 1995. Differentiating the roles of lithology and uplift in the steepening of bedrock river long profiles: an example from southeastern Australia. J. Geol. 103 (2), 227–231. https://doi.org/10.1086/629738.

Goldrick, G., Bishop, P., 2007. Regional analysis of bedrock stream long profiles: evaluation of Hack's SL form, and formulation and assessment of an alternative (the DS form). Earth Surf. Process. Landforms 32 (5), 649–671. https://doi.org/10.1002/esp.1413.

Gross, M., Piller, W.E., 2018. October 23). Fossil glochidia (Bivalvia: unionida: hyriidae) from the middle miocene of western amazonia (Peru). J. Syst. Palaeontol. 17 (13), 1117–1128. https://doi.org/10.1080/14772019.2018.1498034.
Gross, M., Piller, W.E., Ramos, M.I., Douglas da Silva Paz, J., 2011. Late miocene sedimentary environments in South-western amazonia (solimões formation; Brazil). J. S. Am. Earth Sci. 32 (2), 169–181. https://doi.org/10.1016/j.jsames.2011.05.004.
Gruber, S., Peckham, S., 2009. Chapter 7 land-surface parameters and objects in hydrology. Dev. Soil Sci. 3, 171–194. https://doi.org/10.1016/s0166-2481(08)00007-x.
Guilhen, R.F., Scherer, C.M.S., Souza Filho, P.W.M., Dias, M.A., Oliveira, L.E.M., Ferraz, R.P., 2022. Estimation of the Madeira floodplain dynamics from 2008 to 2018. Front. in Water 4, 952810. https://doi.org/10.3389/frwa.2022.952810.
Gupta, S., Pendkar, R., Sarala, C., Reddy, K.M., 2021. Watershed prioritization in GIS: a comparison of multiple approaches. In: Mishra, R.K., Singh, R.B., Dubey, A. (Eds.), Sustainable Climate Action and Water Management. Advances in Geographical and Environmental Sciences. Springer, Singapore. https://doi.org/10.1007/978-981-15-8237-0_4.
Hack, J.T., 1957. Studies of Longitudinal Stream Profile in Virginia and Maryland. US Geol Survey Prof Paper. https://doi.org/10.3133/pp294B, 294-B, 45–97.
Hack, J.T., 1973. Stream-profile analysis and stream-gradient index. J. Res. U. S. Geol. Surv. 1, 421–429.
Hammarstrom, J.M., 2022. Porphyry copper: revisiting mineral resource assessment predictions for the Andes. Minerals 12 (7), 856. https://doi.org/10.3390/min12070856.
Hare, P.W., Gardner, T.W., 1985. Geomorphic indicators of vertical neotectonism along converging plate margins, Nicoya Peninsula, Costa Rica. Tectonic Geomorphol. 4, 75–104.
Hay, W.W., De Conto, R.M., Wold, C.N., Wilson, K.M., et al., 1999. Alternative global Cretaceous paleogeography. In: Barrera, E., Johnson, C.C. (Eds.), Evolution of the Cretaceous Ocean-Climate System. Geological Society of America, pp. 1–47. https://doi.org/10.1130/0-8137-2332-7.1. Special Paper 332.
Hoffman, P.F., 1991. Did the breakout of Laurentia turn gondwanaland inside-out? Sci. 252 (5011), 1409–1412. https://doi.org/10.1126/science.252.5011.1409.
Horton, R.E., 1945. Erosional development of streams and their drainage basins; hydrophysical approach to quantitative morphology. Geol. Soc. Am. Bull. 56 (3), 275. https://doi.org/10.1130/0016-7606.
Hwang, C.L., Yoon, K., 1981. Multiple attribute decision making. In: Lecture Notes in Economics and Mathematical Systems. Springer. https://doi.org/10.1007/978-3-642-48318-9.
Ibanez-Mejia, M., Ruiz, J., Valencia, V.A., Cardona, A., Gehrels, G.E., Mora, A.R., 2011. The Putumayo Orogen of Amazonia and its implications for Rodinia reconstructions: new U–Pb geochronological insights into the Proterozoic tectonic evolution of northwestern South America. Precambrian Res. 191 (1–2), 58–77. https://doi.org/10.1016/j.precamres.2011.09.002.
Internet reference 1: https://earthquake.usgs.gov/earthquakes/map/?extent=-28.22697,-90.04395&extent=-2.76748,-44.07715&range=search&timeZone=utc&search=%7B%22name%22:%22Search%20Results%22,%22params%22:%7B%22starttime%22:%221850-03-16%2000:00:00%22,%22endtime%22:%222022-11-30%2023:59:59%22,%22maxlatitude%22:-4.39,%22minlatitude%22:-26.746,%22maxlongitude%22:-54.141,%22minlongitude%22:-79.98,%22minmagnitude%22:2.5,%22maxmagnitude%22:9,%22orderby%22:%22time%22%7D%7D (Accessed on 30 November, 2022).
Internet reference 2: https://www.world-stress-map.org/(Accessed on 16-March-2023).
Júnior, J.L.S., Tomasella, J., Rodriguez, D.A., 2015. Impacts of future climatic and land cover changes on the hydrological regime of the Madeira River basin. Climatic Change 129 (1–2), 117–129. https://doi.org/10.1007/s10584-015-1338-x.
Kale, V.S., 2010. Reconstruction of late Quaternary fluvio-sedimentary response of Kaveri and Palar rivers: based on chronostratigraphy, digital geomorphometry and remote sensing analysis. J. Quat. Sci. 25 (1), 61–68. https://doi.org/10.1002/jqs.1322.
Kale, V.S., Sengupta, S., Achyuthan, H., Jaiswal, M.K., 2014. Tectonic controls upon Kaveri River drainage, cratonic Peninsular India: inferences from longitudinal profiles, morphotectonic indices, hanging valleys and fluvial records. Geomorphol. 227, 153–165. https://doi.org/10.1016/j.geomorph.2013.07.027.
Keller, E.A., Pinter, N., 2002. Active Tectonics: Earthquakes, Uplift, and Landscape. Prentice Hall.
Kumar, D., Sankar, C.S., 2014. A comparative analysis of TOPSIS and AHP for selection of software development methodology. Proc. Comput. Sci. 46, 1747–1754.
Kumar, P., Sarkar, P., 2022. January 27). A comparison of the AHP and TOPSIS multi-criteria decision-making tools for prioritizing sub-watersheds using morphometric parameters' analysis. Model. Earth Syst. Environ. 8 (3), 3973–3983. https://doi.org/10.1007/s40808-021-01334-x.
Latrubesse, E.M., Cozzuol, M., da Silva-Caminha, S.A., Rigsby, C.A., Absy, M.L., Jaramillo, C., 2010. The late miocene paleogeography of the Amazon basin and the evolution of the Amazon River system. Earth Sci. Rev. 99 (3–4), 99–124. https://doi.org/10.1016/j.earscirev.2010.02.005.
Lee, C.S., Tsai, L.L., 2009. A quantitative analysis for geomorphic indices of longitudinal river profile: a case study of the Choushui River, Central Taiwan. Environ. Earth Sci. 59 (7), 1549–1558. https://doi.org/10.1007/s12665-009-0140-3.
Li, Z., Bogdanova, S., Collins, A., Davidson, A., De Waele, B., Ernst, R., Vernikovsky, V., 2008. Assembly, configuration, and break-up history of Rodinia: a synthesis. Precambrian Res. 160 (1–2), 179–210. https://doi.org/10.1016/j.precamres.2007.04.021.
Lombardo, U., Grützner, C., 2021. Tectonic geomorphology and active faults in the Bolivian Amazon. Global Planet. Change 203, 103544. https://doi.org/10.1016/j.gloplacha.2021.103544.
Mahmood, S.A., Gloaguen, R., 2012. Appraisal of active tectonics in Hindu Kush: insights from DEM derived geomorphic indices and drainage analysis. Geosci. Front. 3 (4), 407–428. https://doi.org/10.1016/j.gsf.2011.12.002.
Mandal, S., Sarkar, S., 2016. Overprint of neotectonism along the course of river chel, north bengal, India. J. Palaeogeogr. 5 (3), 221–240. https://doi.org/10.1016/j.jop.2016.05.004.
Mason, C.C., Romans, B.W., Stockli, D.F., Mapes, R.W., Fildani, A., 2019. Detrital zircons reveal sea-level and hydroclimate controls on Amazon River to deep-sea fan sediment transfer. Geology 47 (6), 563–567. https://doi.org/10.1130/g45852.1.
Mendes, A., Salomão, G., Nogueira, A., Dantas, E., 2015. Provenance of the alter do chão formation in Amazonas state (Itacoatiara-Paritins cities), Amazonas Basin, Brazil. J. S. Am. Earth Sci. 62, 56–69. https://doi.org/10.1016/j.jsames.2015.03.002.
Meshram, S.G., Alvandi, E., Meshram, C., Kahya, E., Fadhil Al-Quraishi, A.M., 2020. January). Application of SAW and TOPSIS in prioritizing watersheds. Water Resour. Manag. 34 (2), 715–732. https://doi.org/10.1007/s11269-019-02470-x.
Nag, S.K., Chakraborty, S., 2003. Influence of rock types and structures in the development of drainage network in hard rock area. J. the Indian Soc. of Remote Sensing 31 (1), 25–35. https://doi.org/10.1007/bf03030749.
Nitheshnirmal, S., Bhardwaj, A., Dineshkumar, C., Rahaman, S.A., 2019. Prioritization of erosion prone micro-watersheds using morphometric analysis coupled with multi-criteria decision making. Multidiscip. Digit. Publ. Institute proc. 24 (1), 11. https://doi.org/10.3390/IECG2019-06207.
Olaya, V., 2009. Chapter 6 basic land-surface parameters. In: Developments in Soil Science. Elsevier, pp. 141–169. https://doi.org/10.1016/s0166-2481(08)00006-8.
Patel, A., Singh, M.M., Singh, S.K., Kushwaha, K., Singh, R., 2022. March 28). AHP and TOPSIS based sub-watershed prioritization and tectonic analysis of ami river basin, Uttar Pradesh. J. Geol. Soc. India 98 (3), 423–430. https://doi.org/10.1007/s12594-022-1995-0.
Pedrera, A., Pérez-Peña, J.V., Galindo-Zaldívar, J., Azañón, J.M., Azor, A., 2009. Testing the sensitivity of geomorphic indices in areas of low-rate active folding (eastern Betic Cordillera, Spain). Geomorphol. 105 (3–4), 218–231. https://doi.org/10.1016/j.geomorph.2008.09.026.
Pfiffner, O.A., Gonzalez, L., 2013. Mesozoic–cenozoic evolution of the western margin of South America: case study of the Peruvian Andes. Geosci. 3 (2), 262–310. https://doi.org/10.3390/geosciences3020262.
Piedade, M.T.F., Junk, W.J., Long, S.P., 2010. A classification of major naturally-occurring amazonian lowland wetlands. Wetlands 30 (4), 677–691. https://doi.org/10.1007/s13157-010-0078-1.
Pike, R., 2000. Geomorphometry - diversity in quantitative surface analysis. Prog. Phys. Geogr. 24 (1), 1–20. https://doi.org/10.1191/030913300674449511.
Pike, R., Evans, I., Hengl, T., 2009. Chapter 1 geomorphometry: a brief guide. Dev. Soil Sci. 3–30 https://doi.org/10.1016/s0166-2481(08)00001-9.
Pingel, H., Strecker, M.R., Alonso, R.N., Schmitt, A.K., 2013. Neotectonic basin and landscape evolution in the eastern cordillera of NW Argentina, humahuaca basin (~24°S). Basin Res. 25 (5), 554–573. https://doi.org/10.1111/bre.12016.
Pinter, N., Keller, E., 1995. Geomorphological analysis of neotectonic deformation, northern Owens Valley, California. Geol. Rundsch. 84 (1), 1–12. https://doi.org/10.1007/bf00192251.
Pourghasemi, H.R., Honarmandnejad, F., Rezaei, M., Tarazkar, M.H., Sadhasivam, N., 2021. March 15). Prioritization of water erosion–prone sub-watersheds using three ensemble methods in Qareaghaj catchment, southern Iran. Environ. Sci. Pollut. Control Ser. 28 (28), 37894–37917. https://doi.org/10.1007/s11356-021-13300-2.
Quiero, F., Tassara, A., Iaffaldano, G., Rabbia, O., 2022. Growth of Neogene Andes linked to changes in plate convergence using high-resolution kinematic models. Nat. Commun. 13 (1), 1–9. https://doi.org/10.1038/s41467-022-29055-4.
Raha, A., Biswas, M., 2022. Quaternary alluvial fan dynamics of the Jaldhaka basin. J. Mt. Sci. 19 (8), 2160–2179. https://doi.org/10.1007/s11629-021-7005-y.
Ramírez-Herrera, M.T., 1998. Geomorphic assessment of active tectonics in the Acambay graben, Mexican Volcanic Belt. Earth Surf. Process. Landforms 23 (4), 317–332. https://doi.org/10.1002/(sici)1096-9837.
Remondo, J., Oguchi, T., 2009. GIS and SDA applications in geomorphology. Geomorphol. 111 (1–2), 1–3. https://doi.org/10.1016/j.geomorph.2009.04.015.
Sarkar, P., Kumar, P., Vishwakarma, D.K., Ashok, A., Elbeltagi, A., Gupta, S., Kuriqi, A., 2022. Watershed prioritization using morphometric analysis by MCDM approaches. Ecol. Inf. 70, 101763 https://doi.org/10.1016/j.ecoinf.2022.101763.
Schepers, G., van Hinsbergen, D.J.J., Spakman, W., Kosters, M.E., Boschman, L.M., McQuarrie, N., 2017. South-American plate advance and forced Andean trench retreat as drivers for transient flat subduction episodes. Nat. Commun. 8 (1) https://doi.org/10.1038/ncomms15249.
Schumm, S.A., 1956. Evolution of drainage systems and slopes in badlands at perth amboy, New Jersey. Geol. Soc. Am. Bull. 67 (5), 597–646. https://doi.org/10.1130/0016-7606.
Seeber, L., Gornitz, V., 1983. River profiles along the Himalayan arc as indicators of active tectonics. Tectonophy. 92 (4), 335–367. https://doi.org/10.1016/0040-1951(83)90201-9.
Smith, A.G., Smith, D.G., Funnell, B.M., 1994. Atlas of Mesozoic and Cenozoic Coastlines. Cambridge University Press, New York, pp. 3–17. ISBN: 0521451558.
Somoza, R., Ghidella, M.E., 2012. Late Cretaceous to recent plate motions in western South America revisited. Earth Planet Sci. Lett. 331, 152–163. https://doi.org/10.1016/j.epsl.2012.02.022.

Strahler, A.N., 1952. Hypsometric (area-altitude) analysis of erosional topography. Geol. Soc. Am. Bull. 63 (11), 1117–1142. https://doi.org/10.1130/0016-7606, 1952.
Strecker, M.R., Hilley, G.E., Arrowsmith, J.R., Coutand, I., 2003. Differential structural and geomorphic mountain-front evolution in an active continental collision zone: the northwest Pamir, southern Kyrgyzstan. Geol. Soc. Am. Bull. 115 (2), 166–181. https://doi.org/10.1130/0016-7606(2003)115<0166:dsagme>2.0.co;2.
Suvires, G.M., Mon, R., Gutiérrez, A.A., 2012. Tectonic effects on the drainage disposition in mountain slopes and Orogen Forelands. A case study: the Central Andes of Argentina. Rev. Bras. Geociencias 42, 229–239. https://doi.org/10.25249/0375-7536.2012421229239.
Torsvik, T.H., 2003. The Rodinia jigsaw puzzle. Science 300 (5624), 1379–1381. https://doi.org/10.1126/science.1083469.
Wallace, T.C., Hall-Wallace, M.K., 2003. Minerals of the Andes: emeralds, gold, and silver from the sky. Rocks Miner. 78 (1), 12–38.
Wang, Y.M., Luo, Y., 2009. On rank reversal in decision analysis. Math. Comput. Model. 49 (5–6), 1221–1229. https://doi.org/10.1016/j.mcm.2008.06.019.
Whipple, K.X., 2004. Bedrock rivers and the geomorphology of active orogens. Annu. Rev. Earth Planet Sci. 32 (1), 151–185. https://doi.org/10.1146/annurev.earth.32.101802.120356.
Williams, H., Hiscott, R.N., 1987. Definition of the Lapetus rift-drift transition in western Newfoundland. Geology 15 (11), 1044. https://doi.org/10.1130/0091-7613(1987)15<1044:dotlrt>2.0.co.
Wołosiewicz, B., 2018. The influence of the deep-seated geological structures on the landscape morphology of the Dunajec River catchment area, Central Carpathians, Poland and Slovakia. Contemp. Trends Geosci. 7, 1–11. https://doi.org/10.2478/ctg-2018-0002.